Role of the organic counterions on the protonation of Strandberg-type phosphomolybdates

Lamine Yaffa, Antoine Blaise Kama, Mohamed Lamine Sall, Cheikh A.K. Diop, Mamadou Sidibé, Michel Giorgi, Mayoro Diop, Romain Gautier

Polyhedron X (2020) X–X

Contents lists available at ScienceDirect

Polyhedron

journal homepage:www.elsevier.com/locate/poly

Role of the organic counterions on the protonation of Strandberg-type phosphomolybdates

Lamine Yaffa,[a]* Antoine Blaise Kama,[a,b]* Mohamed Lamine Sall,[a] Cheikh A. K. Diop,[a] Mamadou Sidibé,[a] Michel Giorgi,[c] Mayoro Diop,[a] Romain Gautier[b]*

[a] *Université Cheikh Anta Diop de Dakar, Facuté des sciences et techniques, Département de Chimie, Laboratoire de Chimie Minérale et Analytique (LA.CHI.MIA), Dakar, Sénégal.*
[b] *Institut des Materiaux Jean Rouxel (IMN), Université de Nantes, CNRS, 2 rue de la Houssinière,BP 32229, 44322 Nantes cedex 3, France.*
[c] *Aix Marseille Univ, CNRS, Centrale Marseille, FSCM, Spectropole Marseille France.*

ARTICLE INFO

Keywords:
Strandberg-type anion
phosphomolybdate
Hydrogen bonds
Organic counterions
Thermal analysis
Cyclic voltametry

ABSTRACT

Strandberg-type phosphomolybdate anions are metal-oxide clusters with general formula $[H_nP_2Mo_5O_{23}]^{(6-n)-}$ (n=0, 1, 2). The protonation / deprotonation of this anion affects its redox properties. Herein, we explain how to select the organic counterions to direct the synthesis towards the non-protonated or protonated anion. The method is illustrated with the synthesis of two new compounds $(C_5H_{16}N_2)_3[P_2Mo_5O_{23}].4H_2O$ (**1**) and $(CH_6N)_4[H_2P_2Mo_5O_{23}].CH_5N.4H_2O$ (**2**). The two compounds were characterized by UV-Visible absorption, IR spectroscopy and single crystal X-ray diffraction. Their thermal stabilities and redox properties were also investigated.

1. Introduction

Polyoxometalates (POMs) are metal-oxide clusters which possess remarkable properties impacting application fields as diverse as catalysis, biology, and medicine [1-7]. Among the diverse structures of POMs, the Strandberg-type anion is described by the connection of five MoO_6 distorted octahedra and two PO_4 distorted tetrahedra. These anions have excellent physical and chemical properties owing to their structural characteristics, as well as their high charges. In addition, the Strandberg anions with the formula $[(RPO_3)_2Mo_5O_{15}]^{4-}$ where "R" are enantiopure organic components, may also present chirality [8]. The chirality can also derive from stereogenic arrangements in the solid state or at the supramolecular level [9-10]. Such chirality is very often reported to be at the origin of optical activity [8-9]. In this article, we focus on the anion with the general formula $[H_nP_2Mo_5O_{23}]^{(6-n)-}$ (n=0, 1, 2). These POMs have small sizes (e.g. 9.0 × 5.6 Å for $[P_2Mo_5O_{23}]^{6-}$) [11], and a relatively high electron density. Yue *et al.* investigated the electronic properties, redox properties, and relative basicity of the terminal oxides of the Strandberg-type POMs. After an analysis of Mulliken charges for the atoms of $[H_nP_2Mo_5O_{23}]^{(6-n)-}$ (n = 0, 1, 2) anions, they concluded that the protonation affects the charge distribution, redox properties and relative stability of the polyanion [12]. Interestingly, Yan *et al.* noted that the changes in the electronic density can modify the redox properties of these POMs [13]. Thus, the reactivity of such clusters depend on either they are protonated or non-protonated (the non-protonated polyanion $[P_2Mo_5O_{23}]^{6-}$ is more prone to be reduced). The size of the counterions or the number of amino groups may also influence the protonation or non-protonation of the final cluster. Therefore, the understanding of supramolecular packing of the POMs with counterions would be important to direct the future synthesis towards protonated or non-protonated clusters.

In this paper, we explain how organic reactants can be appropriately selected to obtain the protonated or non-protonated Strandberg POMs. Through an analysis of previously reported crystal structures in which the Strandberg anions are stabilized with organic counterions, we observed that the non-protonated anions are mainly reported with organic diamines whereas the protonated form is mainly reported with organic monoamines or monoprotonated polyamines. This observation is confirmed and rationalized with the synthesis and characterization of two new compounds $(C_5H_{16}N_2)_3[P_2Mo_5O_{23}].4H_2O$ (**1**) and $(CH_6N)_4[H_2P_2Mo_5O_{23}]$. $CH_5N.4H_2O$ (**2**) from the organic precursors 1,3-pentanediamine and methylamine, which are commonly used in the synthesis of organic or hybrid materials (at 25°C: for 1,3-pentanediamine, pka1 = 10.97, pka2 = 8.92; for methylamine, pka = 10.66) [14-17].

2. Experimental section

2.1. Materials

Molybdenum oxide (85%), methylamine (40%), phosphoric acid (85%), and 1,3-pentanediamine (98%) were purchased from Sigma-Aldrich and used without further purification with distilled water.

* Corresponding author.
E-mail addresses: kama.antoineblaise@yahoo.fr (A.B. Kama)
Romain.Gautier@cnrs-imn.fr (R. Gautier).

2.2 Synthesis

For $(C_5H_{16}N_2)_3[P_2Mo_5O_{23}].4H_2O$ (**1**) , one pot synthesis was carried out by dissolving molybdenum oxide (0.288g, 2 mmol), 1,3-pentanediamine (0.204g, 2 mmol) and phosphoric acid (0.392g, 4 mmol) in water (30 ml).

For $(CH_6N)_4[H_2P_2Mo_5O_{23}].CH_5N.4H_2O$ (**2**) one pot synthesis was carried out by dissolving molybdenum oxide (0.288 g, 2 mmol), methylamine (0.311 g, 4 mmol) and phosphoric acid (0.196 g, 2 mmol) in water (30 ml). The solutions were heated under reflux and stirred for two hours. Colourless crystals suitable for X-ray diffraction were obtained after slow evaporation.

2.3 X-ray diffraction

For compound (**1**), single-crystal X-ray diffraction data were collected with a Bruker-Nonius Kappa CCD diffractometer (MoKα radiation λ=0.71073 Å). The crystal to detector distance was 60 mm. Absorption corrections were considered using SADABS [18]. The determination was carried out using direct methods [19]. The crystal structures including the anisotropic displacement parameters were refined with SHELXL-2013[20]. PLATON [21] was used to check additional symmetry elements and Crystallographic Information Files were compiled with Olex2.12.

For compound (**2**), single-crystal X-ray diffraction data were measured on a Rigaku Oxford Diffraction SuperNova diffractometer at the MoKα radiation. Data collection reduction and multiscan ABSPACK correction were performed with CrysAlisPro (Rigaku Oxford Diffraction). The crystal structures including the anisotropic displacement parameters were refined with SHELXL- 2013 [20]. PLATON [21] was used to check additional symmetry elements and Crystallographic Information Files were compiled with Olex2.12. Crystallographic data are summarized in table 1.

2.4 Spectroscopy

The UV-Visible absorption spectra were recorded using a Thermo Scientific GENESYS 10S UV-Vis spectrophotometer between 200 nm and 700 nm at room temperature in aqueous solution. For compound (**1**), 15 mg was solubilized in 10ml of distilled water. For compound (**2**), 45 mg was used in the same conditions. Distilled water was used as blank.

IR spectroscopy measurements were carried out for both compounds. IR measurements were performed using ATR (Attenuated Total Reflectance) method from 4000 to 400 cm^{-1} [22].

2.5 TG/DSC measurements

Thermogravimetric (TG) and Differential Scanning Calorimetry (DSC) measurements were carried out with a Setaram Sensys Evo under Argon flow, from room temperature to 800 °C, with a heating rate of 5 °C/min.

2.6 Electrochemical measurements

The electrochemical proprieties of compounds (**1**) and (**2**) were investigated in aqueous acid medium (0.1 M HCl) with a scan rate of 5 mV/s. The electrochemical measurements with different scanning rate from 5 mV/s to 50 mV/s were performed in the same conditions.

Table 1. Crystal data and structure refinement for compounds (**1**) and (**2**).

	1	**2**
Molecular formula	$(C_5H_{16}N_2)_3[P_2Mo_5O_{23}].4H_2O$	$(CH_6N)_4[H_2P_2Mo_5O_{23}].CH_5N.4H_2O$
Formula weight	1294.27	1143.03
Crystal color, habit	Plate, colorless	Plate, colorless
Crystal system	Monoclinic,	Triclinic
a, Å	30.9409(2)	11.0064(1)
b, Å	15.1427(1)	11.3360(1)
c, Å	20.9747(2)	13.8994(2)
α, deg	90	107.361(1)
β, deg	125.007(1)	103.355(1)
γ, deg	90	95.240(1)
V, $Å^3$	8049.32 (13)	1586.28(3)
Space group	*C2/c*	*P*–1
Z	1	7
F(000)	597	1120
θ range, deg	6.4–25.7	2.8–28.6
Absorption coefficient, mm^{-1}	0.32	0.213
T, K	293	293
λ, Å	0.71073	0.71073
Reflections collected	52772	83877
Independent reflections	6961 [R(int)= 0.053]	7439 [R(int)= 0.059]
Final R indices	R1=0.028, wR2=0.081	R1=0.026 , wR2 = 0.069
GOF on F^2	1.14	1.05
Peak, hole /e$Å^{-3}$	-0.69 , −1.41	-0.76−0.80

3. Results and discussion

3.1 Synthesis

The starting materials play a fundamental role to obtain Strandberg type polyoxometalate clusters [23-24]. The self-assembly of appropriate ions from the starting materials with the removal of water molecules will lead to the Strandberg clusters. The general reaction of Rolf Strandberg for this type of POMs is given as [24]:

$$_pH^+ + _qMoO_4^{2-} + _rHPO_4^{2-} \rightleftharpoons (H^+)_p(MoO_4^{2-})_q(HPO_4^{2-})_r$$

With excess phosphate ions, the main complexes are $(H^+)_8(MoO_4^{2-})_5(HPO_4^{2-})_2$, $(H^+)_9(MoO_4^{2-})_5(HPO_4^{2-})_2$, $(H^+)_{10}(MoO_4^{2-})_5(HPO_4^{2-})_2$. The removal of water lead respectively to $P_2Mo_5O_{23}^{6-}$, $P_2Mo_5O_{23}^{5-}$, $H_2P_2Mo_5O_{23}^{4-}$.

For compound (**1**), the self-assembly of the starting materials namely molybdenum oxide (MoO_3), phosphoric acid (H_3PO_4), 1,3-pentanediamine ($C_5H_{14}N_2$) and water (H_2O) (pH =1. 71) leads to $[P_2Mo_5O_{23}]^{6-}$ building block.

For compound (**2**) the self-assembly of the starting materials namely molybdenum oxide (MoO_3), phosphoric acid (H_3PO_4), methylamine (CH_5N) and water (H_2O) (pH = 4.85) leads to $[H_2P_2Mo_5O_{23}]^{4-}$ building block.

3.2 Structure description

Single-crystal X-ray diffraction performed on a crystal of compound (**1**) reveals that it crystallizes in monoclinic system (space group *C2/c*). The asymmetric unit contains one anion, three cations and four water molecules (Fig. 1). Single-crystal X-ray diffraction performed on a crystal of compound (**2**) reveals that it crystallizes in a triclinic system (space group *P*-1). The asymmetric unit contains one anion, four cations, four water molecules and one neutral amine (Fig. 1).

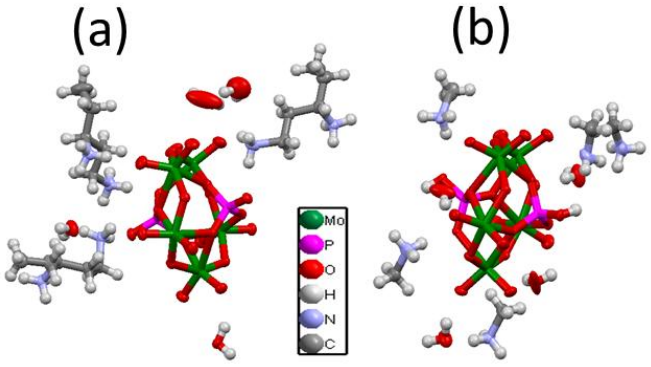

Fig. 1. Asymmetric unit of (a) compound (**1**) and (b) compound (**2**)

Both compounds (**1**) and (**2**) are built with diphosphopentamolybdate anions $[H_nP_2Mo_5O_{23}]^{(6-n)-}$. Such anions are built upon five MoO_6 octahedra and two PO_4 tetrahedra. The octahedra form a pentagonal ring by sharing four edges and one corner. The two PO_4 tetrahedra have three oxygen atoms in common with the ring (Fig.2). The difference between the anions of (**1**) and (**2**) lies on the protonation: the anion of (**1**) is non-protonated whereas the anion of (**2**) is protonated. There are four types of Mo-O bonds for each anion: (a) Mo-O_t, with O_t = terminal oxygen atoms (bond lengths range = 1.686(3) –1.725(3) Å for compound (**1**) and 1.699(2)–1.712(2) Å for compound (**2**)) ; (b) Mo-O_{b1}, with O_{b1} = oxygen atoms shared by two molybdenum atoms (bond lengths range = 1.883(3) –1.979(3) Å for compound (**1**) and 1.8846(19)–1.9432(18) Å for compound (**2**)); (c) Mo-O_{b2}, with O_{b2} = oxygen atoms shared by phosphorus and molybdenum atoms, (bond lengths range= 2.224(3)– 2.240(3) Å for compound (**1**) and 2.2923(18)–2.3138(19) Å for compound (**2**)); (d) Mo-O_{b3}, with O_{b3} = oxygen atoms shared by two molybdenum atoms and one phosphorus atom (bond lengths range = 2.190(3)–2.399(3) Å for compound (**1**) and 2.2098(17)–2.3874(16) Å for compound (**2**)). The P–O distances range from 1.512(3) to 1.550(3) Å for compound (**1**) and 1.5169(18) to 1.5518(18) Å for compound 2. In each compound, the anion, cation and water molecules are interacting through strong hydrogen bonds. In compound (**1**), two neighboring clusters are connected via hydrogen bonds by one bridging (…H-N-H…O-H…) or two bridging (…H-N-H…O-H… and …H-N-$(CH_2)_3$-N-H…) while in compound (**2**) two neighboring clusters are connected via hydrogen bonds by two or three bridging (…H-N-H…O-H…) (fig.2).

For the stabilization of the Strandberg clusters, one needs to consider the charge balance with the organic cations and steric effects. Through an analysis of the literature, one can observe that the non-protonated Strandberg clusters are commonly obtained with diammonium cations as counterions (e.g. $(C_2H_{10}N_2)_3[P_2Mo_5O_{23}].6H_2O$, $[(C_4N_2H_{12})_3][P_2Mo_5O_{23}].H_2O$, $[(C_3N_2H_{12})_3][P_2Mo_5O_{23}].4H_2O$, or $(H_2bpp)_3[P_2Mo_5O_{23}]$) [25-28], while the protonated form is obtained with monoamonium or polyamine for which only one amine group is protonated (e.g. $(C_4H_{12}N)_4[H_2P_2Mo_5O_{23}].5H_2O$,

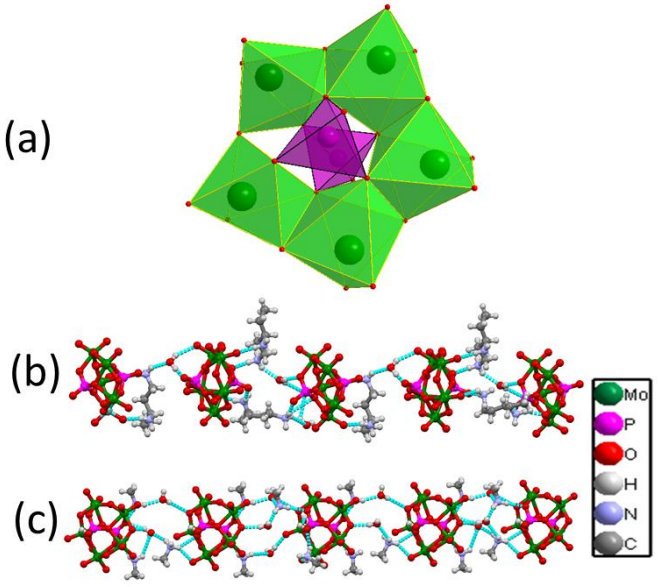

Fig. 2. Representation of (a) the Strandberg polyanion; and the supramolecular arrangements of (b) compounds (**1**) and (c) (**2**) (Hydrogen bonds are represented in blue dotted line).

$(C_6H_{14}N)_5[HP_2Mo_5O_{23}]\cdot 4H_2O$, $(C_4H_7N_2)_4[HP_2Mo_5O_{23}].H_3O\cdot 4.5H_2O$) [12, 28, 29]. For the non-protonated anion, three organic diammonium or six organic monoammonium molecules would be necessary to counterbalance the charge. Six organic monoammonium molecules around the anion would lead to strong steric effects. To prevent such steric effects, the non-protonated anion must be stabilized with diammonium cations. On the other hand, monoammonium cations can stabilize protonated anions. The pKa of precursors bases (1,3-pentanediamine and methylamine) do not influence the deprotonation of the Strandberg cluster. Thus, both bases have very similar

pKa (at 25°C: for 1, pKa1 = 10.97, pKa2 = 8.92; for 2, pKa = 10.66), but the POM of compound (**1**) is fully deprotonated whereas the POM of compound (**2**) is diprotonated. As the non-protonated form exhibits the most interesting catalytic properties, this analysis is interesting for the future design of diphosphomolybdate Strandberg type anions.

3.3 UV and IR spectroscopy

The UV–Visible absorption of both compound (**1**) & (**2**) was analysed in the 200–700 nm range in aqueous solution. The UV spectra reveal one absorption peak at 267 nm and 257 nm for compounds (**1**) and (**2**), respectively (Fig. 3). This absorption band is attributed to the pπ–dπ charge transfer transitions of the O → Mo bonds [29, 30]. It is interesting to note that there is small shift between the two absorption peaks. This may be due to the protonation of the compound 2; indeed, such protonation affects the charge distribution and subsequently the electronic density.

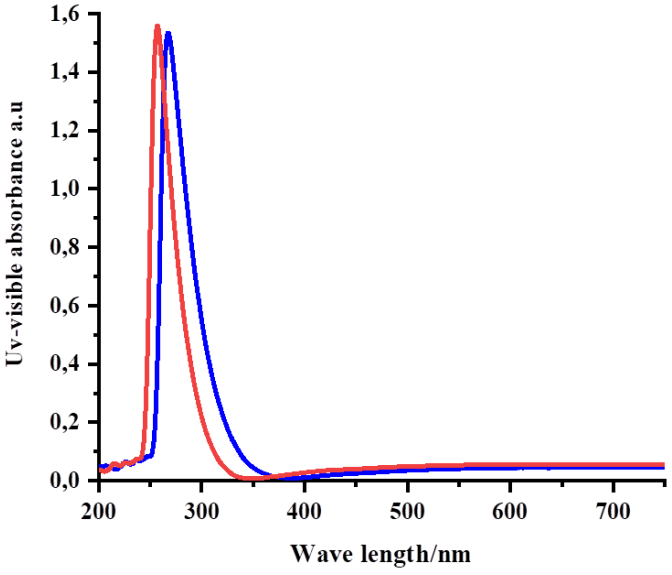

Fig. 3. UV-Visible absorption of compounds (**1**) (blue colour) and (**2**) (red colour).

The IR-spectra of compounds (**1**) and (**2**) (Fig. S1) can be divided into two regions. The first region ranging from 4000 to 1100 cm^{-1} is attributed to the vibrations of water molecules and organic ligands and the second region from 1100 to 400 cm^{-1} contains bands attributed to the POM vibrations. Thus, the characteristic bands at 938 cm^{-1}, 908 cm^{-1}, 673 cm^{-1}, 590 cm^{-1} and 506 cm^{-1} for compound (**1**); 993 cm^{-1}, 929 cm^{-1}, 874 cm^{-1}, 686 cm^{-1} and 650 cm^{-1} for compound (**2**) are ascribed to υ(Mo=O) and υ(Mo–O–Mo) [31, 32].

The peaks in the range 1100–1020 cm^{-1} are affiliated to the characteristic vibrations of ν(P–O) [31]. The range 3500–2800 cm^{-1} shows many peaks ascribed to O–H stretching of water molecules, as well as N–H and C–H stretching vibrations. Bands between 1650 and 1100 cm^{-1} are associated to O–H bending of water molecules, and N–H and C–H bending vibrations. The frequencies between 1530 and 1340 cm^{-1} are assigned to the C–N and C–C stretching vibrations of the organic part. There is a slight shift for the cluster bands in compound (**2**) as compared to compound (**1**) which is consistent with the bond lengths observed in the crystal structures.

3.4 TG/DSC analysis

In order to examine the thermal stability, TG and DSC analyses of both compounds were carried out from room temperature to 800 °C (fig. 4). The TG data for compound (**1**) shows four mass losses. The first loss of 5 % between 30 and 100 °C would correspond to the loss of the water molecules (calculated loss: 5 %). The second weight loss of 8% between 100 and 200 °C can be attributed to the decomposition of six NH_3 (calculated loss: 7 %). In this range, the DSC curve shows another endothermic peak. The third weight loss of 19 % between 200 to 330 °C corresponds to fifteen CH_4 (calculated loss: 18 %). The last loss starting from 330 °C corresponds to the degradation of the cluster. The total weight loss observed is 45 %.

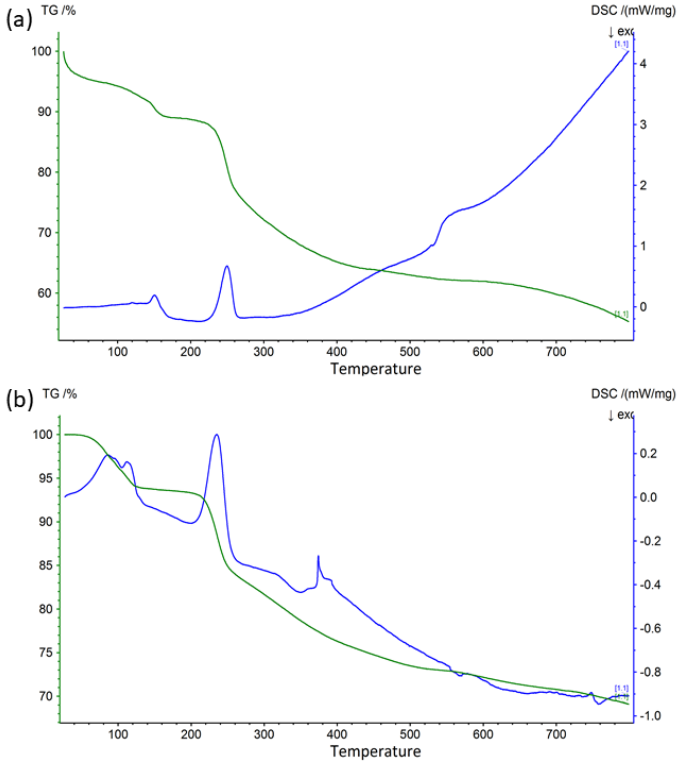

Fig. 4. Thermogravimetric analysis and differential scanning calorimetry of (a) compound (**1**) and (b) compound (**2**).

The TG curve for compound (**2**) exhibits three steps for the mass loss. The first loss between 30 and 180 °C of 7 % corresponds to the loss of four water molecules (calculated loss: 6 %). The DSC curve shows an endothermic peak in this range. The second loss of 13 % (calculated 14 %) between 180 and 340 °C corresponds to the organoamines degradation (five CH_3NH_2). In this range, the DSC curve shows one endothermic peak. The last loss starting from 340 °C corresponds to the cluster degradation. The total observed weight loss is 31 %.

3.5 Electrochemical properties

The results of cyclic voltammetry of compounds (**1**) and (**2**) in the range -300 mV to 700 mV are represented in fig. 5. The cyclic voltammetry were performed in 0.1M HCl because the reduction of POMs is not expected to be favored in aprotic solvents, since it would result in an increase of the negative charge of the complex. In protic solvents, the transfer of electrons is accompanied by the transfer of protons such that the negative charge of the complex does not change [33, 34]. This proton transfer is not expected to influence the redox potential because the negative charge of the complex is not affected. On the other hand, to transform the non-protonated version to the protonated version of Strandberg POMs, a change of charge (then a change of the charge distribution) is necessary. Therefore, the redox properties are affected.

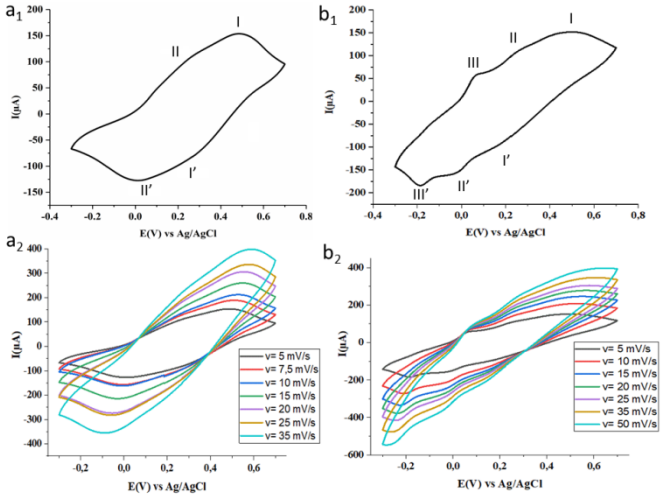

Fig. 5. Electrochemical measurements of compounds (a) (**1**) and (b) (**2**) ($_1$: Cyclic voltammograms in 0.1 M HCl at scan rate = 5 mV/s, $_2$: Cyclic voltammograms in 0.1 M HCl with different scan rates).

For compound (**1**), two reversible redox peaks are observed and the mean peak potentials $E_{1/2}$ = (Epa + Epc)/2 are 390 mV (I-I') and 140 mV (II-II') corresponding to two consecutive one electron processes [29]. For compound (**2**), three reversible redox peaks are observed and the mean peaks potentials are 335 mV (I-I'); 135 mV (II-II'); -65 mV (III-III') respectively. The three redox peaks correspond to three consecutive one electron processes [35]. We performed the oxidation and reduction of the two complexes with different scanning speeds (Fig. 5). An increase in the intensity of the oxidation and reduction peaks with the increase of the scanning speed is observed. The mean peak potentials of compound (**1**) are higher than the ones of compound (2). Thus, the oxidizing power of (1) is higher than (**2**) confirming that compound (**1**) is more prone to be reduced.

For the two compounds we have noted a linear increase in the anodic and cathodic peaks with the square root of the scanning speed which characterizes a redox diffusion-controlled process phenomenon fig. 6 [36, 37]. Cyclic voltammograms of 1,3 pentanediammonium dichloride and methylammonium chloride were also measured in the same conditions. No peak could be observed (see supporting information Fig. S2). All these results show that the redox properties of the Strandberg type anions can be maintained in our compounds.

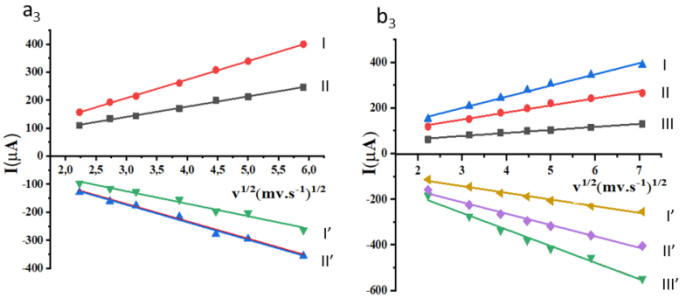

Fig.6. Calibration curve for peak currents with respect to the square root of the scanning speed.

4. Conclusion

Two Strandberg type phosphomolybdates anions with different organic counterions were synthetized. The crystal structure of compound (**1**) consists of the non-protonated Strandberg anion stabilized with a diammonium cation (1,3-pentanediaminium), while the compound (**2**) consists of the protonated Strandberg anion stabilized with a monoammonium (methylaminium). Through the analysis of our compounds and previously reported structures, we demonstrated that using a diamine as precursor more likely lead to the non-protonated Strandberg anion, while other amines more likely lead to the protonated version of the Strandberg anion.

Declaration of Competing Interest

The authors declared that there is no conflict of interest.

Acknowledgements

We thank the French embassy for financial support as part of the program "Appui à la recherche France-Sénégal».

Appendix A. Supplementary data

CCDC <2008961> contains the supplementary crystallographic data for (1) <2008962> contains the supplementary crystallographic data for (2). These data can be obtained free of charge via http://www.ccdc.cam.ac.uk/conts/retrieving.html, or from the Cambridge Crystallographic Data Centre, 12 Union Road, Cambridge CB2 1EZ, UK; fax: (+44) 1223-336-033; or e-mail: deposit@ccdc.cam.ac.uk.

5. References

[1] C. L. Hill, Guest Editor; Chem. Rev. **1998**, 98, 1.

[2] A. Srinivasa Rao, T. Arumuganathan, V. Shivaiah, S. K. Das, J. Chem. Sci. **2011**, 123, 229–239.

[3] I. A. Weinstock, R. E. Schreiber, R. Neumann, Chem. Rev. **2018**, 118, 2680.

[4] J. J. Walsh, A.M. Bond, R. J. Forster, T.E. Keyes. Coord. Chem. Rev. **2016**, 306, 217.

[5] J. J. Baldoví, S. Cardona-Serra, A. Gaita-Ariño, E. Coronado, Adv. Inorg. Chem., **2017**, 69, 213.

[6] Z. J. Liu, X. L.Wang, C. Qin, Z. M. Zhang, Y. G. Li, W. L. Chen, E. B. Wang, Coord. Chem. Rev. **2016**, 313, 94.

[7] X. L. Chen, Y. Zhou, V.A.L. Roy, S. T. Han, Adv. Mater. **2018**, 30, 1703950.

[8] M. Carraro, A. Sartorel, G. Scorrano, C. Maccato, M. H. Dickman, U. Kortz, M. Bonchio, Angew. Chem. Int. Ed. **2008**, 47, 7275–7279.

[9] Y. Wang, S. Pan, H. Yu, X. Su, M. Zhang, F. Zhanga, J. Han, Chem. Commun. **2013**, 49, 306–308.

[10] B. Hasenknopf, K. Micoine, E. Lacôte, S. Thorimbert, M. Malacria, R. Thouvenot, Eur. J. Inorg. Chem. **2008**, 5001–5013.

[11] J. l. Liang, M. M. Wu, P. H. Wei, J. C. Zhao, H. Huang, C. F. Li, Y. K. Lu, Y. Q. Liu, C. G. Liu, J. Catal. **2018**, 358, 155–167.

[12] S. M. Yue, L. K. Yan, Z. M. Su, G. H. Li, Y. G. Chen, J. F. Ma, H. B. Xu, H. J. Zhang J. Coord. Chem. **2004**, 57, 123–132.

[13] L. K. Yan, Z. M. Su, K. Tan, M. Zhang, L. Y. Qu, R. S. Wang, Int. J. Quantum Chem. **2005**, 105, 37.

[14] R. Tingley, V. Bertolasi, K. Vaughan, J. Chem. Crystallogr. **2005**, 35, 821–828.

[15] S. Lu, J. Peng, J. Wu, C. Li, X. Cao, H. Gu, Chem. Commun. **2016**,52**,** 760–763.

[16] N. S. Draskovic, D. D. Radanovic, U. Rychlewska, B. Warzajtis, I. M. Stanojevic, M. I. Djuran, Polyhedron. **2012**, 43, 185–193.

[17] J. Yang, T. Qin, L. Xie, K. Liao, T. Li, F. Hao, J. Mater. Chem. C, **2019**,7, 10724–10742.

[18] G. M. Sheldrick, SADABS, University of Göttingen, Germany, **2002**.

[19] M. C. Burla, R. Caliandro, M. Camalli, B. Carrozzini, G.L. Cascarano, L. De Caro, C. Giacovazzo, G. Polidori, R. Spagna, J. Appl. Crystallogr. **2005**, 38, 381.

[20] G. M. Sheldrick, SHELXL-2013, University of Göttingen, Germany, **2013**.

[21] A. L. Spek, PLATON, Utrecht University, The Netherlands, **2001**.

[22] FT-IR Spectroscopy-Attenuated Total Reflectance (ATR). Perkin Elmer Life and Analytical Sciences **2005**.

[23] C. Wang, J. Shi, K, Yu, B. Zhou, J. Coord. Chem. **2018**, 71, 3970-3979.

[24] R. Strandberg, Acta Chemica Scandinavica **1973**, 27, 1004–1018.

[25] S. V. Ganesan, S. Natarajan, J. Chem. Sci. **2005**, 117, 219–226.

[26] M. Asnani, D. Kumar, T. Duraisamy, A. Ramanan J. Chem. Sci. **2012**, 124, 1275–1286.

[27] H. Liu, H.Wang, D. Niu, Z. Lu, Synth. Reac. Inorg. Met. Org. Nano-Met. Chem. **2007**, 37, 103.

[28] A. Aranzabe, A. S. J. Wéry, S. Martin, J. M. Gutiérrez-Zorrilla, A. Luque, M. Martınez-Ripoll, P. Roman, Inorg. Chim. Acta **1997**, 255, 35–45.

[29] A. Harchani, A. Haddad, Z. Anorg. Allg. Chem. **2017**, 643, 1744–1751.

[30] M. Ayed, I. Nagazi, B. Ayed, A. Haddad, J. Clust. Sci. **2012,** 23, 1133–1142.

[31] Y. Ma, Y. Lu, E. Wang, X. Xu, Y. Guo, X. Bai, L. Xu, J. of Mol . Struct. **2006**, 784, 18–23.

[32] Y. Wang, L. C. Zhang, Z. M. Zhu, N. Li, A. F. Deng, S. Y. Zheng, Transition Met. Chem. **2011**, 36, 261–267.

[33] B. Sarr, A. Mbaye, C. A. K. Diop, M. Sidibe, F. Melin, P. Hellwig, F. Maury, F. Senocq, P. Guionneau, M. Giorgi, R. Gautier, Inorg. Chim. Acta **2019**, 491, 84–92.

[34] M. Sadakane, E. Steckhan, Chem. Rev. **1998**, 98, 219.

[35] S. Shi, L. Chen, X. Zhao, B. Ren, X. Cui, J. Zhang, Inorg. Chim. Acta **2018**, 482, 870–877.

[36] W. T. Dai, L. P. cui, K. Yu, J. H. Lv, X. Y. Ma, B. B. Zhou, J. Solid State Chem. **2020,** 288, 121399.

[37] X. Wang, Z. Kang, E. Wang, C. Hu, J. Electroanal. Chem. **2002,** 523, 142–149.